Available online at www.sciencedirect.com
ScienceDirect
Journal of Sound and Vibration 323 (2009) 194–213
JOURNAL OF SOUND AND VIBRATION
www.elsevier.com/locate/jsvi

Model identification and order response prediction for bladed wheels

X. Sheng*

Applied Mechanics, Technical Centre, Cummins Turbo Technologies Co. Ltd., St Andrew's Road, Huddersfield, West Yorkshire HD1 6RA, UK

Received 22 January 2008; received in revised form 25 October 2008; accepted 8 December 2008
Handling Editor: C.L. Morfey
Available online 18 January 2009

Abstract

A method is proposed in this paper for model identification and order response prediction for bladed wheels. This method makes use of measured blade tip-to-blade tip frequency response functions of a mistuned wheel and assumes responses of the wheel subject to order excitations to be a weighted sum of a number, which is equal to the number of the blades, of modes of the corresponding tuned wheel. The model for the mistuned wheel is identified in terms of the scale-reduced mass and stiffness matrices from which an expression for order responses is derived. The method is validated by comparing order responses calculated using this method with those from the original equation for two wheel models, a lumped parameter model and a finite element paddle wheel model. It can be concluded that, using this method, resonance responses of a mistuned wheel to order excitations at and around the natural frequencies of the first family can be accurately predicted, even mistuning is large. From the order responses the strain levels in the blades can be evaluated and the suitability for the wheel to be released for field use can be assessed.

1. Introduction

Bladed wheels are generally designed to be a cyclically symmetric structure. In reality however, due to casting process, machining tolerances and non-uniform wear in services, there are always variations in geometry and material property between blades. This phenomenon is called mistuning and a bladed wheel having mistuning is a mistuned wheel. Mistuning is random in nature and unavoidable in practice.

For a cyclically symmetric (or tuned) structure consisting of N identical sectors, vibration modes can be grouped [1] by the nodal-diameter (ND) number n, where $n = 0,1,2,\ldots N/2$ if N is even or $n = 0,1,2,\ldots(N-1)/2$ if N is odd. In terms of a cylindrical coordinate system, the mode shapes, $\mathbf{u}^r$ and $\mathbf{u}^{r+1}$, of the rth and $(r+1)$th sectors are related by $\mathbf{u}^{r+1} = e^{in2\pi/N}\mathbf{u}^r$ for the n-ND modes, where $i = \sqrt{-1}$. This shows a travelling wave pattern which extends to all the sectors. A natural frequency associating with a ND number different from zero and $N/2$ (where N is even) repeats itself. Rotating in a housing and subject to aerodynamic excitations,

*Tel.: +44 1484 832522; fax: +44 1484 832310.
E-mail address: xiaozhen.sheng@cummins.com

0022-460X/$ - see front matter © 2008 Elsevier Ltd. All rights reserved.
doi:10.1016/j.jsv.2008.12.008

the blades have the same vibration amplitude. For a cyclically symmetric structure, dynamic analysis can be performed using a single sector with degrees of freedom much less than the whole structure [2].

The presence of mistuning in a bladed wheel generally invalidates those tuned dynamic features. A mistuned wheel may exhibit vibration localisation and amplification, in which few blades have responses much greater than those of other blades and the tuned response (the response of the corresponding tuned wheel under the same order excitation). As a result, mistuning not only significantly reduces the high cycle fatigue (HCF) life of the wheel, but also makes it difficult to predict (due to the lack of knowledge of actual properties of the blades) or measure (due to not knowing which blade in which wheel is the most responsive) the representative response. Those mistuning effects are observed not only on large bladed-disks found in aero-engines, but also on small radial turbine wheels used in turbochargers. Since the latter are manufactured by casting and machining, mistuning is produced more possibly by blade-to-blade variations in material property.

To predict the response of an individual mistuned wheel, parameters (material properties and blade geometries) specific to this wheel must be known and they are different, although in general not significantly, from the design or tuned values. Thus mistuning identification has been and will still be an important research topic. Mistuning may be investigated from a statistical point of view due to its random nature. Statistical quantities, such as mean, standard deviation and even distribution, may be produced from responses of a large number of wheel samples of the same design and production. This requires calculations and/or measurements to be carried out for up to several thousands times. Such a task cannot be accomplished by either measurement or using conventional numerical methods (normally the finite element method (FEM)) which model the whole wheel with too many degrees of freedom. This has provoked another research topic, i.e. computationally efficient modelling for mistuned wheels. The response of a wheel is a nonlinear function of wheel parameters. Since a tuned wheel has repeated natural frequencies and mistuning is a perturbation to this tuned system, it may be expected that the response of the wheel does not continuously change when the wheel parameters change from the designed, tuned point. This observation has brought in the idea of intentional mistuning, in hope that the unwanted effect of random, uncontrollable mistuning is depressed to a required extent by the intentional, controllable mistuning.

Mistuning in bladed wheels has been studied for over 30 years in order to resolve some of the aforementioned issues. A recent (up to 2005) and thorough review can be found in Ref. [3]. Different techniques have been developed to produce an order-reduced model. Refs. [4–6] represent a mistuned system using a lumped parameter model consisting of masses and springs. Such a model has a high computational efficiency and is useful to qualitatively investigate mistuning effect, but difficult to predict stresses and strains which are the main concern in HCF of the mistuned wheel. Refs. [7–9] model a mistuned system using the Component Mode Synthesis technique in which the first few modes, which are produced using FEM, of each sector (substructure) of the system are employed to capture vibration of the whole system. In addition to the sub-structural modes of a mistuned system, the modes of the corresponding tuned system (called tuned modes) have also been used to synthesise the vibration of the mistuned system [10]. Ref. [11] combines recipes in the above two approaches, introducing a method which makes use of both tuned system modes and blade component modes to generate an order-reduced model. Other efficient modelling approaches are also attempted, see e.g. [12,13].

Though statistics may be performed using an order-reduced model, mistuning identification for individual mistuned wheels is still appealing. Mistuning is identified normally from some, often inadequate, measured data, leaving the problem indeterminate. To obtain a set of unique parameters (these parameters can be blade mass matrices, blade stiffness matrices and blade frequencies, etc.), extra conditions must be assumed. Two mistuning identification methods are suggested in Refs. [14,15] in which blades are represented by multi-mass-spring systems coupled with each other and the hub is rigid and fixed. The first, termed *the random modal stiffness approach* (RMS), assumes mistuning exists in the stiffness matrices of the blades only. It is further assumed that the mistuned modal shapes are not significantly different from the tuned ones. Under such conditions, the mistuned stiffness matrix of a blade can be determined straightforwardly by measuring *all* the mistuned blade frequencies (not the bladed disk system frequencies). The second is termed *the maximum likelihood* (ML) *approach*. In this approach, both the mass and stiffness matrices of a blade are allowed to be mistuned. By assuming a joint probability density function (PDF) for the stiffness and mass matrices, the mistuned mass and stiffness matrices are estimated under the condition that they give the measured blade

frequencies while at the same time make the PDF maximum. It is illustrated that the ML approach works better than the RMS approach in terms of the mean and standard deviation of the maximum forced response of the blades subject to order excitations. The difficulty in using the ML approach is how to choose correctly the type of the joint PDF and its parameters. It is also a fact that this method is based on the blade alone frequencies which may not be measurable if the blades cannot be removed from the hub as in turbocharger turbine wheels.

Another mistuning identification method, presented in Refs. [16,17], is based on the fundamental mistuning model developed in Ref. [13]. There are four assumptions in the fundamental mistuning model: (a) only a single, isolated family of modes will be excited; (b) the strain energy of that family's modes is primarily in the blades; (c) the family's natural frequencies are closely spaced; and finally (d) mistuning is small. There is another assumption in the model which is not stated explicitly: modes in this family can be approximated by a weighted sum of a number of tuned modes. Based on these assumptions, a number of approximations are also made in the derivation of the model and the mistuning identification method, which may further limit their usefulness. To identify mistuning, the mistuned frequencies and modal shapes of that family must be measured. Mistuning is identified in terms of sector frequency deviations which are specially defined. Once the mistuning is determined, the model can be used to predict responses to order excitations which mainly excite that family of modes.

Mistuning effects such as vibration localisation and amplification are demonstrated in some of the aforementioned references e.g. Refs. [3,9]. The phenomenon of vibration localisation is interpreted in a review paper [18] using the stability theory and in Ref. [19] using the transfer matrix approach. Ref. [20] discusses the phenomenon of vibration localisation induced by a crack on a single blade based on a simple wheel model. It is numerically demonstrated in Ref. [21] that intentional mistuning may be used to depress some of the negative effects of the random mistuning. Though efforts are made in Ref. [21] to explore the mechanism of intentional mistuning, a satisfactory explanation has not yet been achieved. A possible route to this may be the use of singular value decomposition, as shown in Ref. [22].

A bladed wheel is normally operated at high speeds and in a high temperature gas field. The effect of temperature can be easily accounted for by properly changing material's Young's modulus. Centrifugal and Coliolis forces generated from the wheel rotation may have some impact on the effect of mistuning though they are generally neglected in previous research. Centrifugal forces may increase (stiffening) or reduce (softening) the natural frequencies of a non-rotating wheel. In current industrial practices, a scaling factor is given to the material's Young's modulus to account for the combined effect of gas temperature and centrifugal forces, while no consideration is given to the Coliolis effect. The effect of Coliolis forces on mistuned wheel vibration has been demonstrated recently in Ref. [23].

This paper presents a method for model identification and order response prediction for bladed assemblies, especially for small turbocharger turbine wheels in which the blades and the hub are integrated. This method makes use of measured blade tip-to-blade tip frequency response functions of a mistuned wheel and assumes responses of the wheel subject to order excitations to be a weighted sum of a number equal to the number of the blades of modes of the corresponding tuned wheel. The effect of wheel rotation will not be included in this paper. Detailed formulations of the method are presented in Section 2. Validations of the method are conducted in Section 3 by comparing order responses calculated using the proposed method and those from the original equation for a mass-spring bladed wheel model and a FE paddle wheel model. From these results, conclusions are drawn in Section 4.

2. Model identification and mistuned order responses

2.1. Order reduction of equation of motion

The FE equation of motion of a mistuned bladed wheel of N blades may be written as

$$(\mathbf{M}_0 + \Delta\mathbf{M})\ddot{\mathbf{x}} + (\mathbf{K}_0 + \Delta\mathbf{K})\mathbf{x} = \tilde{\mathbf{Q}}e^{i\omega t}, \tag{1}$$

where matrices $\mathbf{M}_0$ and $\mathbf{K}_0$ represent the mass and stiffness matrices of the tuned counterpart, $\Delta\mathbf{M}$ and $\Delta\mathbf{K}$ describe changes in the mass and stiffness matrices due to mistuning, and $\tilde{\mathbf{Q}}e^{i\omega t}$ is an order excitation at radian

frequency ω. An *order excitation* is a loading configuration in which each blade is subject to a pressure distribution over the blade surface. The pressure distributions are harmonic temporally at the same frequency. The amplitude magnitude of the pressure distribution on a blade is identical to those on other blades but phase difference between any pair of consecutive blades is equal to an integer, n, times the angle $(2\pi/N)$ between these two blades. The integer n is termed the *excitation order*. At the nth order, excitation frequency $\omega = n\Omega$, where Ω is the wheel rotation speed in radians per second. Order excitations are generated from the Fourier harmonics of the pressure field of the housing. The scale of Eq. (1) is normally large and may be reduced by expressing mistuned vibration as a weighted sum of a number of N tuned modes, as done in Ref. [13], i.e.

$$\mathbf{x} = [\boldsymbol{\varphi}_1\boldsymbol{\varphi}_2, \ldots, \boldsymbol{\varphi}_N]\boldsymbol{\beta}e^{i\omega t} = \boldsymbol{\Phi}\boldsymbol{\beta}e^{i\omega t}, \tag{2}$$

where $\boldsymbol{\Phi} = [\boldsymbol{\varphi}_1\boldsymbol{\varphi}_2, \ldots, \boldsymbol{\varphi}_N]$ is a matrix formed by $\boldsymbol{\varphi}_j$ ($j = 1,2,\ldots,N$) which are modes of the tuned system and $\boldsymbol{\beta}$ is the vector of the weights. $\mathbf{M}_0$, $\mathbf{K}_0$, $\boldsymbol{\Phi}$ and the corresponding natural frequencies can be calculated using FEM from the tuned, designed wheel model. In Fig. 1, natural frequencies of a typical turbine wheel (Fig. 2) with 13 blades are calculated under free–free condition and plotted against ND numbers (from 0 to 6). That the free–free condition is used is due to the wheel is supported by a floating journal bearing through a small shaft. Lines are drawn to connect natural frequencies of the same order at different ND numbers, forming families of modes. The number of modes in a family is equal to the number of blades, since the natural frequencies corresponding to ND numbers 1 to 6 repeat themselves. Although the frequencies in the first family (the lowest line) are not necessarily close to each other due to different vibrations of the hub for different ND numbers (for the 0ND, the hub vibrates torsionally and for the 1ND the hub vibrates translationally), they are much lower than the second natural frequency of any ND number.

For a mistuned wheel, the concept of ND number cannot strictly apply. However, vibration modes can still be grouped into families each containing N modes (see Section 3). For conventional turbochargers with a vane-less housing, the modes in the first family are most concerned since resonant vibration at the natural frequencies of these modes are greatest and often lead to high cycle fatigue failure. Therefore order responses of the blades at these frequencies must be accurately predicted, so that whether the wheel can be released for field use can be assessed. An assumption has been made in writing Eq. (2) that the mistuned vibration forced by the order excitation $\tilde{\mathbf{Q}}e^{i\omega t}$ is still within the sub-space spanned by the chosen tuned modes. By doing so, the mistuned wheel under the order excitation is approximated as a dynamic system having N degrees of freedom. Since the resonant vibration at the mistuned natural frequencies of the first family is concerned and differences between frequencies in this family and those in other families are large, the N tuned modes in Eq. (2) may be

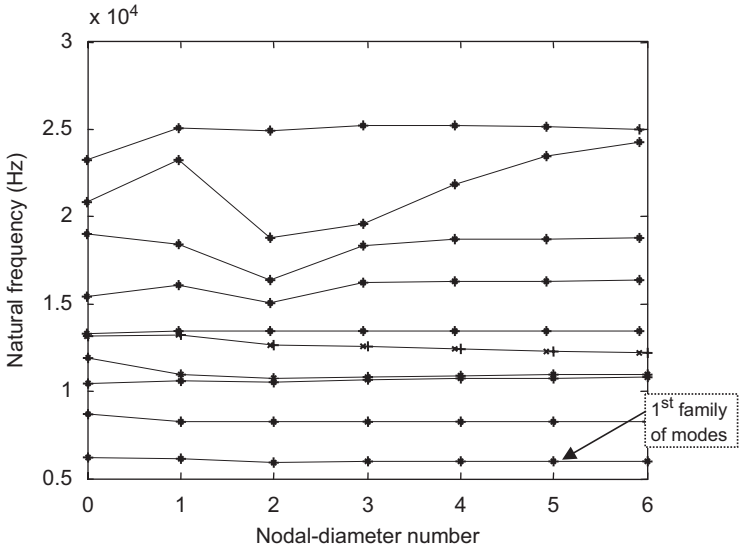

Fig. 1. Natural frequencies of a typical turbine wheel with 13 blades.

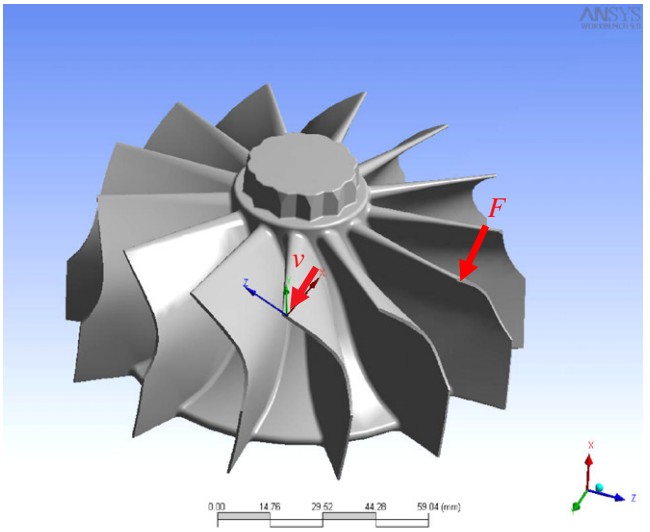

Fig. 2. Measurement of blade tip-to-blade tip frequency response functions.

chosen to be the modes in the first family (Fig. 1) of the tuned wheel. The accuracy of doing so is demonstrated in Section 3.

In what follows, no further assumption or approximation are introduced; this is different from the method proposed in Refs. [16,17] where, in addition to Eq. (2), a number of approximations are made. Substituting Eq. (2) into Eq. (1) and pre-multiplying $\mathbf{\Phi}^{\mathrm{T}}$, yields

$$-\omega^2(\mathbf{M}^* + \mathbf{\Phi}^{\mathrm{T}}\Delta\mathbf{M}\mathbf{\Phi})\boldsymbol{\beta} + (\mathbf{K}^* + \mathbf{\Phi}^{\mathrm{T}}\Delta\mathbf{K}\mathbf{\Phi})\boldsymbol{\beta} = \mathbf{\Phi}^{\mathrm{T}}\tilde{\mathbf{Q}}, \tag{3}$$

where $\mathbf{M}^* = \mathbf{\Phi}^{\mathrm{T}}\mathbf{M}_0\mathbf{\Phi}$ and $\mathbf{K}^* = \mathbf{\Phi}^{\mathrm{T}}\mathbf{K}_0\mathbf{\Phi}$ are diagonal matrices formed by the modal masses and stiffness of the tuned system. If $\mathbf{\Phi}^{\mathrm{T}}\Delta\mathbf{M}\mathbf{\Phi}$ and $\mathbf{\Phi}^{\mathrm{T}}\Delta\mathbf{K}\mathbf{\Phi}$ are known, then forced vibration can be determined by solving Eq. (3). The task of *model identification* here is to estimate $\mathbf{\Phi}^{\mathrm{T}}\Delta\mathbf{M}\mathbf{\Phi}$ and $\mathbf{\Phi}^{\mathrm{T}}\Delta\mathbf{K}\mathbf{\Phi}$, rather than $\Delta\mathbf{M}$ and $\Delta\mathbf{K}$ themselves (estimation of $\Delta\mathbf{M}$ and $\Delta\mathbf{K}$ should be termed mistuning identification). The matrices $\mathbf{\Phi}^{\mathrm{T}}\Delta\mathbf{M}\mathbf{\Phi}$ and $\mathbf{\Phi}^{\mathrm{T}}\Delta\mathbf{K}\mathbf{\Phi}$ are of order $N \times N$ and symmetric, therefore the determination of them do not require a large number of measurements for small radial turbocharger turbine wheels, since blades on a wheel are not too many.

2.2. Model identification

Model and mistuning identifications can be performed only when some measured data are available. Measured data can be natural frequencies and modal shapes of the mistuned system. Here, use is made of blade tip-to-blade tip frequency response functions. To do so, frequency response functions are measured for blade tips. In the measurement, the force and response are required to be applied and measured at a blade tip and in the direction normal to the blade surface (Fig. 2). A matrix of order $N \times N$, denoted by $\tilde{\mathbf{H}}(\omega)$ and termed the *blade tip-to-blade tip frequency response matrix*, is formed by these functions. This matrix is symmetric. For a small radial turbocharger turbine wheel, the number of blades is not too large (e.g. 12), and the measurement of matrix $\tilde{\mathbf{H}}(\omega)$ can be completed relatively quickly by making use of the symmetry of this matrix. Using the modal testing technique [24], the measurements may be further reduced down to a single row or column of elements in $\tilde{\mathbf{H}}(\omega)$. When using this technique however, special cautions must be excised owing to the fact that for a mistuned wheel (this is definitely the case for a tuned wheel, see Introduction), some natural frequencies may be very close, or even identical, to each other.

Now define the force vector of the rth order excitation in which the forces are applied at the blade tips and normal to the blade surfaces:

$$\mathbf{F}(t) = (\mathrm{e}^{\mathrm{i}r\alpha_1}, \mathrm{e}^{\mathrm{i}r\alpha_2}, \ldots, \mathrm{e}^{\mathrm{i}r\alpha_N})^{\mathrm{T}}\mathrm{e}^{\mathrm{i}\omega t} = \tilde{\mathbf{F}}\mathrm{e}^{\mathrm{i}\omega t}, \tag{4}$$

where $\alpha_j = 2\pi j/N$ is the azimuth angle of the jth blade. The global force vector, $\tilde{\mathbf{Q}}$, in Eq. (3) can be generated accordingly. The normal displacement amplitudes of the tips due to this special order excitation can be calculated from the measured tip-to-tip frequency response matrix $\tilde{\mathbf{H}}(\omega)$, using

$$\tilde{\mathbf{q}} = \tilde{\mathbf{H}}\tilde{\mathbf{F}}, \tag{5}$$

where $\tilde{\mathbf{q}} = (\tilde{q}^{(1)}, \tilde{q}^{(2)}, \ldots, \tilde{q}^{(N)})^{\mathrm{T}}$ is the vector of the normal tip displacement amplitudes.

The tip displacement vector of the sth blade is denoted by $(\tilde{u}^{(s)}, \tilde{v}^{(s)}, w^{(s)})^{\mathrm{T}}$. According to Eq. (2),

$$\begin{Bmatrix} \tilde{u}^{(s)} \\ \tilde{v}^{(s)} \\ \tilde{w}^{(s)} \end{Bmatrix} = \sum_{m=1}^{N} \beta_m \begin{Bmatrix} \varphi_{1m}^{(s)} \\ \varphi_{2m}^{(s)} \\ \varphi_{3m}^{(s)} \end{Bmatrix}, \tag{6}$$

where $\varphi_{1m}^{(s)}$, $\varphi_{2m}^{(s)}$ and $\varphi_{3m}^{(s)}$ are the x-, y- and z-components of the tip displacement of the s^{th} blade in the mth tuned mode. Now the unit vector normal to the blade surface at the blade tip is denoted by $\mathbf{a}^{(s)}$, and from Eq. (6)

$$\mathbf{a}^{(s)T} \begin{Bmatrix} \tilde{u}^{(s)} \\ \tilde{v}^{(s)} \\ \tilde{w}^{(s)} \end{Bmatrix} = \sum_{m=1}^{N} \beta_m \mathbf{a}^{(s)T} \begin{Bmatrix} \varphi_{1m}^{(s)} \\ \varphi_{2m}^{(s)} \\ \varphi_{3m}^{(s)} \end{Bmatrix}. \tag{7}$$

In Eq. (7), the term on the left hand side is the normal displacement of the tip, $\tilde{q}^{(s)}$. Denoting

$$a_{sm} = \mathbf{a}^{(s)\mathrm{T}}(\varphi_{1m}^{(s)}, \varphi_{2m}^{(s)}, \varphi_{3m}^{(s)})^{\mathrm{T}}, \tag{8}$$

then Eq. (7) becomes

$$\sum_{m=1}^{N} a_{sm}\beta_m = \tilde{q}^{(s)} \quad \text{or} \quad \mathbf{A}\boldsymbol{\beta} = \tilde{\mathbf{q}}, \tag{9}$$

where $\mathbf{A}$ is a $N \times N$ matrix with a_{sm} being the normal displacement of the sth tip in the mth tuned mode. From Eqs. (9) and (5), $\boldsymbol{\beta}$ can be expressed as

$$\boldsymbol{\beta} = \mathbf{A}^{-1}\tilde{\mathbf{q}} = \mathbf{A}^{-1}\tilde{\mathbf{H}}\tilde{\mathbf{F}}. \tag{10}$$

Using Eq. (10), $\boldsymbol{\beta}$ can be calculated for different excitation frequencies and orders. Particularly, for excitation frequencies, ω_1 and ω_2, and for a number of, N, order excitations defined by

$$\tilde{\mathbf{F}}_j = (\mathrm{e}^{\mathrm{i}r_j\alpha_1}, \mathrm{e}^{\mathrm{i}r_j\alpha_2}, \ldots, \mathrm{e}^{\mathrm{i}r_j\alpha_N})^{\mathrm{T}}, \tag{11}$$

where $j = 1,2,\ldots,N$ and r_j are excitation orders, two $N \times N$ matrices are produced following Eq. (10)

$$\mathbf{B}_1 = \mathbf{A}^{-1}\tilde{\mathbf{H}}(\omega_1)[\tilde{\mathbf{F}}_1, \tilde{\mathbf{F}}_2, \ldots, \tilde{\mathbf{F}}_N], \tag{12a}$$

$$\mathbf{B}_2 = \mathbf{A}^{-1}\tilde{\mathbf{H}}(\omega_2)[\tilde{\mathbf{F}}_1, \tilde{\mathbf{F}}_2, \ldots, \tilde{\mathbf{F}}_N]. \tag{12b}$$

If the global force vector corresponding to $\tilde{\mathbf{F}}_j$ is denoted by $\tilde{\mathbf{Q}}_j$, then Eq. (3) gives

$$[-\omega_1^2(\mathbf{M}^* + \boldsymbol{\Phi}^{\mathrm{T}}\Delta\mathbf{M}\boldsymbol{\Phi}) + (\mathbf{K}^* + \boldsymbol{\Phi}^{\mathrm{T}}\Delta\mathbf{K}\boldsymbol{\Phi})]\mathbf{B}_1 = \boldsymbol{\Phi}^{\mathrm{T}}[\tilde{\mathbf{Q}}_1, \tilde{\mathbf{Q}}_2, \ldots, \tilde{\mathbf{Q}}_N], \tag{13a}$$

$$[-\omega_2^2(\mathbf{M}^* + \boldsymbol{\Phi}^{T}\Delta\mathbf{M}\boldsymbol{\Phi}) + (\mathbf{K}^* + \boldsymbol{\Phi}^{\mathrm{T}}\Delta\mathbf{K}\boldsymbol{\Phi})]\mathbf{B}_2 = \boldsymbol{\Phi}^{\mathrm{T}}[\tilde{\mathbf{Q}}_1, \tilde{\mathbf{Q}}_2, \ldots, \tilde{\mathbf{Q}}_N], \tag{13b}$$

from which $\boldsymbol{\Phi}^{\mathrm{T}}\Delta\mathbf{M}\boldsymbol{\Phi}$ and $\boldsymbol{\Phi}^{\mathrm{T}}\Delta\mathbf{K}\boldsymbol{\Phi}$ can be determined:

$$\boldsymbol{\Phi}^{\mathrm{T}}\Delta\mathbf{M}\boldsymbol{\Phi} = -\mathbf{M}^* + \frac{1}{\omega_2^2 - \omega_1^2}\boldsymbol{\Phi}^{\mathrm{T}}\{[\tilde{\mathbf{Q}}_1, \tilde{\mathbf{Q}}_2, \ldots, \tilde{\mathbf{Q}}_N](\mathbf{B}_1^{-1} - \mathbf{B}_2^{-1})\}, \tag{14a}$$

$$\boldsymbol{\Phi}^{\mathrm{T}}\Delta\mathbf{K}\boldsymbol{\Phi} = -\mathbf{K}^* + \frac{1}{\omega_2^2 - \omega_1^2}\boldsymbol{\Phi}^{\mathrm{T}}\{[\tilde{\mathbf{Q}}_1, \tilde{\mathbf{Q}}_2, \ldots, \tilde{\mathbf{Q}}_N](\omega_2^2\mathbf{B}_1^{-1} - \omega_1^2\mathbf{B}_2^{-1})\}. \tag{14b}$$

With the insertion of Eq. (12) into Eq. (14) yields

$$\mathbf{\Phi}^{\mathrm{T}}\Delta\mathbf{M}\mathbf{\Phi} = -\mathbf{M}^{*} + \frac{1}{\omega_2^2-\omega_1^2}\{\mathbf{\Phi}^{\mathrm{T}}[\tilde{\mathbf{Q}}_1,\tilde{\mathbf{Q}}_2,\ldots,\tilde{\mathbf{Q}}_N]\}[\tilde{\mathbf{F}}_1,\tilde{\mathbf{F}}_2,\ldots,\tilde{\mathbf{F}}_N]^{-1}\{\tilde{\mathbf{H}}^{-1}(\omega_1)-\tilde{\mathbf{H}}^{-1}(\omega_2)\}\mathbf{A}, \tag{15a}$$

$$\mathbf{\Phi}^{\mathrm{T}}\Delta\mathbf{K}\mathbf{\Phi} = -\mathbf{K}^{*} + \frac{1}{\omega_2^2-\omega_1^2}\{\mathbf{\Phi}^{\mathrm{T}}[\tilde{\mathbf{Q}}_1,\tilde{\mathbf{Q}}_2,\ldots,\tilde{\mathbf{Q}}_N]\}[\tilde{\mathbf{F}}_1,\tilde{\mathbf{F}}_2,\ldots,\tilde{\mathbf{F}}_N]^{-1}\{\omega_2^2\tilde{\mathbf{H}}^{-1}(\omega_1)-\omega_1^2\tilde{\mathbf{H}}^{-1}(\omega_2)\}\mathbf{A}. \tag{15b}$$

Being the global force vector corresponding to $\tilde{\mathbf{F}}_j$ defined in Eq. (11), $\tilde{\mathbf{Q}}_j$ may be expressed as

$$\tilde{\mathbf{Q}}_j = \begin{Bmatrix} \mathrm{e}^{\mathrm{i}r_j\alpha_1}\mathbf{a}^{(1)} \\ \mathrm{e}^{\mathrm{i}r_j\alpha_2}\mathbf{a}^{(2)} \\ \vdots \\ \mathrm{e}^{\mathrm{i}r_j\alpha_N}\mathbf{a}^{(N)} \\ 0 \\ \vdots \\ 0 \end{Bmatrix}, \tag{16}$$

and

$$\mathbf{\Phi}^{\mathrm{T}}\tilde{\mathbf{Q}}_j = \begin{Bmatrix} \mathbf{\varphi}_1^{\mathrm{T}} \\ \mathbf{\varphi}_2^{\mathrm{T}} \\ \vdots \\ \mathbf{\varphi}_N^{\mathrm{T}} \end{Bmatrix}\tilde{\mathbf{Q}}_j, \tag{17}$$

where

$$\mathbf{\varphi}_m^{\mathrm{T}}\tilde{\mathbf{Q}}_j = [\varphi_{1m}^{(1)},\varphi_{2m}^{(1)},\varphi_{3m}^{(1)},\varphi_{1m}^{(2)},\varphi_{2m}^{(2)},\varphi_{3m}^{(2)},\ldots,\varphi_{1m}^{(N)},\varphi_{2m}^{(N)},\varphi_{3m}^{(N)},\ldots]\begin{Bmatrix} \mathrm{e}^{\mathrm{i}r_j\alpha_1}\mathbf{a}^{(1)} \\ \mathrm{e}^{\mathrm{i}r_j\alpha_2}\mathbf{a}^{(2)} \\ \vdots \\ \mathrm{e}^{\mathrm{i}r_j\alpha_N}\mathbf{a}^{(N)} \\ 0 \\ \vdots \\ 0 \end{Bmatrix},$$

or

$$\mathbf{\varphi}_m^{\mathrm{T}}\tilde{\mathbf{Q}}_j = \mathrm{e}^{\mathrm{i}r_j\alpha_1}\mathbf{a}^{(1)T}\begin{Bmatrix} \varphi_{1m}^{(1)} \\ \varphi_{2m}^{(1)} \\ \varphi_{3m}^{(1)} \end{Bmatrix} + \mathrm{e}^{\mathrm{i}r_j\alpha_2}\mathbf{a}^{(2)T}\begin{Bmatrix} \varphi_{1m}^{(2)} \\ \varphi_{2m}^{(2)} \\ \varphi_{3m}^{(2)} \end{Bmatrix} + \cdots + \mathrm{e}^{\mathrm{i}r_j\alpha_N}\mathbf{a}^{(N)T}\begin{Bmatrix} \varphi_{1m}^{(N)} \\ \varphi_{2m}^{(N)} \\ \varphi_{3m}^{(N)} \end{Bmatrix}.$$

According to Eq. (8),

$$\mathbf{\varphi}_m^{\mathrm{T}}\tilde{\mathbf{Q}}_j = (a_{1m},a_{2m},\ldots,a_{Nm})\tilde{\mathbf{F}}_j. \tag{18}$$

Thus

$$\mathbf{\Phi}^{\mathrm{T}}[\tilde{\mathbf{Q}}_1,\tilde{\mathbf{Q}}_2,\ldots,\tilde{\mathbf{Q}}_N] = \mathbf{A}^{\mathrm{T}}[\tilde{\mathbf{F}}_1,\tilde{\mathbf{F}}_2,\ldots,\tilde{\mathbf{F}}_N]. \tag{19}$$

Substitution of Eq. (19) into Eq. (15) gives

$$\mathbf{\Phi}^{\mathrm{T}}\Delta\mathbf{M}\mathbf{\Phi} = -\mathbf{M}^{*} + \frac{1}{\omega_2^2-\omega_1^2}\mathbf{A}^{\mathrm{T}}\{\tilde{\mathbf{H}}^{-1}(\omega_1)-\tilde{\mathbf{H}}^{-1}(\omega_2)\}\mathbf{A}, \tag{20a}$$

$$\mathbf{\Phi}^{\mathrm{T}}\Delta\mathbf{K}\mathbf{\Phi} = -\mathbf{K}^{*} + \frac{1}{\omega_2^2-\omega_1^2}\mathbf{A}^{\mathrm{T}}\{\omega_2^2\tilde{\mathbf{H}}^{-1}(\omega_1)-\omega_1^2\tilde{\mathbf{H}}^{-1}(\omega_2)\}\mathbf{A}. \tag{20b}$$

Now let $\omega_1 = \omega$, $\omega_2 = \omega + \Delta\omega$, then Eq. (20a) becomes

$$\mathbf{\Phi}^{\mathrm{T}}\Delta\mathbf{M}\mathbf{\Phi} = -\mathbf{M}^* + \frac{1}{(2\omega + \Delta\omega)\Delta\omega}\mathbf{A}^{\mathrm{T}}\{\tilde{\mathbf{H}}^{-1}(\omega) - \tilde{\mathbf{H}}^{-1}(\omega + \Delta\omega)\}\mathbf{A},$$

which gives the following equation after letting $\Delta\omega \to 0$

$$\mathbf{\Phi}^{\mathrm{T}}\Delta\mathbf{M}\mathbf{\Phi} = -\mathbf{M}^* - \frac{1}{2\omega}\mathbf{A}^{\mathrm{T}}\frac{\mathrm{d}\tilde{\mathbf{H}}^{-1}(\omega)}{\mathrm{d}\omega}\mathbf{A}. \tag{21a}$$

Similarly from Eq. (20b),

$$\mathbf{\Phi}^{\mathrm{T}}\Delta\mathbf{K}\mathbf{\Phi} = -\mathbf{K}^* + \mathbf{A}^{\mathrm{T}}\left(\tilde{\mathbf{H}}^{-1}(\omega) - \frac{\omega}{2}\frac{\mathrm{d}\tilde{\mathbf{H}}^{-1}(\omega)}{\mathrm{d}\omega}\right)\mathbf{A}. \tag{21b}$$

Eq. (21) gives an estimation of matrices $\mathbf{\Phi}^{\mathrm{T}}\Delta\mathbf{M}\mathbf{\Phi}$ and $\mathbf{\Phi}^{\mathrm{T}}\Delta\mathbf{K}\mathbf{\Phi}$ which, together with others, define the order-reduced model for the mistuned wheel (see Eq. (3)). They are determined by the chosen tuned modes and the tip-to-tip FRF matrix only. As shown in this equation, the estimated $\mathbf{\Phi}^{\mathrm{T}}\Delta\mathbf{M}\mathbf{\Phi}$ and $\mathbf{\Phi}^{\mathrm{T}}\Delta\mathbf{K}\mathbf{\Phi}$ are in general dependant on frequency. Their dependences on the excitation frequency are explained by the fact that the mistuned vibration is not exactly spanned by the chosen tuned modes. However, if

$$\tilde{\mathbf{K}}(\omega) = \mathbf{A}^{\mathrm{T}}\tilde{\mathbf{H}}^{-1}(\omega)\mathbf{A}, \tag{22}$$

can be expressed as

$$\tilde{\mathbf{K}}(\omega) = \mathbf{C} - \omega^2\mathbf{D}, \tag{23}$$

where $\mathbf{C}$ and $\mathbf{D}$ are equivalent stiffness and mass matrices of order $N \times N$, then Eq. (21) gives $\mathbf{\Phi}^{\mathrm{T}}\Delta\mathbf{M}\mathbf{\Phi}$ and $\mathbf{\Phi}^{\mathrm{T}}\Delta\mathbf{K}\mathbf{\Phi}$ which are independent of frequency. Here $\tilde{\mathbf{K}}(\omega)$ may be termed *the equivalent dynamic stiffness matrix*.

2.3. Order response prediction

Using the identified model matrices given in Eq. (21), order responses of the mistuned wheel can be predicted using Eqs. (3) and (2). It can be shown that Eq. (3) now becomes

$$[\mathbf{A}^{\mathrm{T}}\tilde{\mathbf{H}}^{-1}(\omega)\mathbf{A}]\boldsymbol{\beta} = \mathbf{\Phi}^{\mathrm{T}}\tilde{\mathbf{Q}}, \tag{24}$$

or

$$\boldsymbol{\beta} = [\mathbf{A}^{-1}\tilde{\mathbf{H}}(\omega)\mathbf{A}^{-\mathrm{T}}]\mathbf{\Phi}^{\mathrm{T}}\tilde{\mathbf{Q}}, \tag{25}$$

and Eq. (2) gives

$$\mathbf{x} = \mathbf{\Phi}[\mathbf{A}^{-1}\tilde{\mathbf{H}}(\omega)\mathbf{A}^{-\mathrm{T}}]\mathbf{\Phi}^{\mathrm{T}}\tilde{\mathbf{Q}}\mathrm{e}^{\mathrm{i}\omega t}. \tag{26}$$

This is an estimation of the order response of the wheel. It can be seen from Eq. (24) that when the excitation frequency satisfies

$$\det(\tilde{\mathbf{H}}^{-1}(\omega)) = 0 \tag{27}$$

then resonance occurs. In other words, the natural frequencies of the mistuned wheel can be exactly recovered from the identified model.

The accuracy of Eq. (26) is demonstrated in the following section. The accuracy of Eq. (26) may also be indicated by the extent to which the equivalent dynamic stiffness defined in Eq. (22) can be approximated by Eq. (23) in the frequency range containing the mistuned natural frequencies in the first family.

3. Results

The method proposed in previous sections is tested in this section by comparing order responses calculated using this method (i.e. Eq. (26), the tip-to-tip frequency response functions are computed using the original equation Eq. (1)) and those calculated directly from the original equation (i.e. Eq. (1)). Two bladed wheel

models are examined; one is a lumped parameter model with 13 blades and the other is a finite element paddle wheel model with 12 blades. Comparisons are presented here for the 6th order response only, since mistuning effects are found to be more prominent for this order for wheels with 12 or 13 blades [25].

3.1. For a lumped parameter model

The lumped parameter model is shown in Fig. 3. The bladed wheel is modelled as a rigid disk connecting a number, N ($N=13$), of 2-mass-4-spring systems representing the blades. The jth blade is represented by masses m_{aj} and m_{bj} and springs of stiffness k_{aj}, k_{bj}, k_{cj} and k_{dj}. The position of the jth blade is described by an angle α_j measured from a reference radius. The distances from m_{aj} and m_{bj} to the disk centre are R_a and R_b, respectively. A spring (not shown in the figure) of stiffness k_{ej} is present to couple the first stage mass, m_{aj}, of the jth blade and that of the $(j+1)$th blade. The disk is described by mass M and inertial moment J. The disk is subject to stiffness, k_x and k_y in the horizontal and vertical directions with $k_x=k_y=k$. The model has $4N+3$ degrees of freedom. The tangential and radial displacements of m_{aj} relative to the disk are denoted by x_{aj} and y_{aj} and those of m_{bj} by x_{bj} and y_{bj}. Observed from the ground, the displacements of the mass centre of the disk in the x- and y-directions are denoted by x and y and the rotation angle of the disk by θ. Various acceleration components (centrifugal acceleration and Coliolis acceleration, etc.) of, and forces (external forces are not shown) applied by the springs on, mass m_{sj} (where $s=a,b$) are depicted in Fig. A1 (see Appendix A). Based on this figure, the differential equations of the model can be derived by applying Newton's second law to all the blade masses and to the disk for its translational motions, and the momentum moment law to the disk for its rotational vibration. These differential equations are listed in Appendix A.

Now let

$$\mathbf{x}=(x,y,\theta,x_{a1},y_{a1},x_{b1},y_{b1},x_{a2},y_{a2},x_{b2},y_{b2},\ldots,x_{aN},y_{aN},x_{bN},y_{bN})^{\mathrm{T}}. \tag{28}$$

The equations of motion of the model can be written as

$$\mathbf{M}\ddot{\mathbf{x}}+\mathbf{K}\mathbf{x}=\mathbf{Q}(t), \tag{29}$$

where $\mathbf{M}$ is the mass matrix and $\mathbf{K}$ the stiffness matrix. $\mathbf{Q}(t)$ is the externally applied force vector. It is assumed that in the nth order excitation, the blade masses, m_{aj} and m_{bj}, are subject to forces, $P_a e^{in\alpha_j}e^{i\omega t}$ and $P_b e^{in\alpha_j}e^{i\omega t}$, respectively, in the tangential direction. Thus $\mathbf{Q}(t)=\tilde{\mathbf{Q}}e^{i\omega t}$, where

$$\tilde{\mathbf{Q}}=(0,0,0\vdots P_a e^{in\alpha_1},0,P_b e^{in\alpha_1},0\vdots P_a e^{in\alpha_2},0,P_b e^{in\alpha_2},0\vdots\cdots\vdots P_a e^{in\alpha_N},0,P_b e^{in\alpha_N},0)^{\mathrm{T}}. \tag{30}$$

Used parameters for the tuned wheel are listed in Table 1. A loss factor of 0.005 has been estimated for all the springs to account for material damping. Mistuning is generated from a normal distribution for the first stage

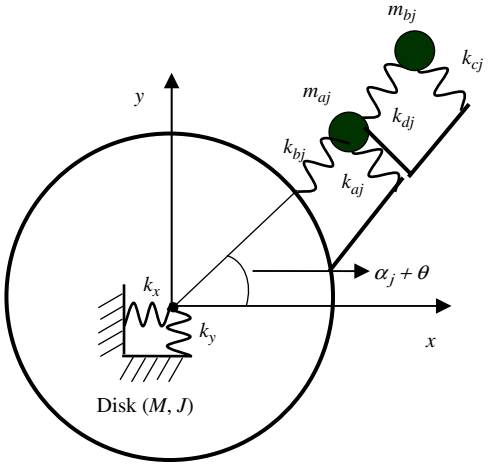

Fig. 3. A lumped parameter model.

Table 1
Parameters for the tuned wheel.

Disk mass, M	0.078 kg
Disk inertia moment, J	0.0038 kg m^2
Radii, R_a, R_b	0.21 m, 0.22 m
Disk stiffness, $k_x = k_y$	4.556×10^7 N/m
Fist stage blade mass, m_a	5.248×10^{-4} kg
Second stage blade mass, m_b	$m_a/2$
Fist stage tangential blade stiffness, k_a	1×10^6 N/m
First stage radial blade stiffness, k_b	$5 \times k_a$
Second stage tangential blade stiffness, k_c	$0.5 \times k_a$
Second stage radial blade stiffness, k_d	$0.5 \times k_b$
Blade coupling stiffness, k_e	$k_a/10$

Table 2
Parameters for the mistuned wheel.

Blade number	Fist stage blade mass, m_a ($\times 10^{-4}$ kg)	Fist stage tangential blade stiffness, k_a ($\times 10^6$ N/m)	Blade coupling stiffness, k_e ($\times 10^5$ N/m)
1	5.166	1.051	1.090
2	4.406	1.169	1.073
3	5.383	1.059	1.058
4	4.694	0.936	1.000
5	5.991	1.038	1.068
6	4.825	0.899	1.057
7	5.525	0.998	0.974
8	5.363	0.995	0.962
9	4.764	1.000	0.970
10	4.109	0.968	0.852
11	5.217	1.110	0.977
12	4.718	0.813	1.012
13	5.570	1.043	1.031

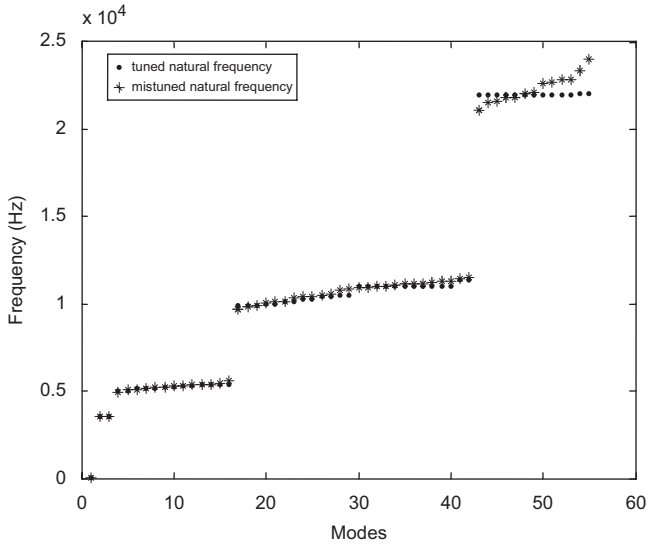

Fig. 4. Natural frequencies of the tuned (dot) and mistuned (star) wheels.

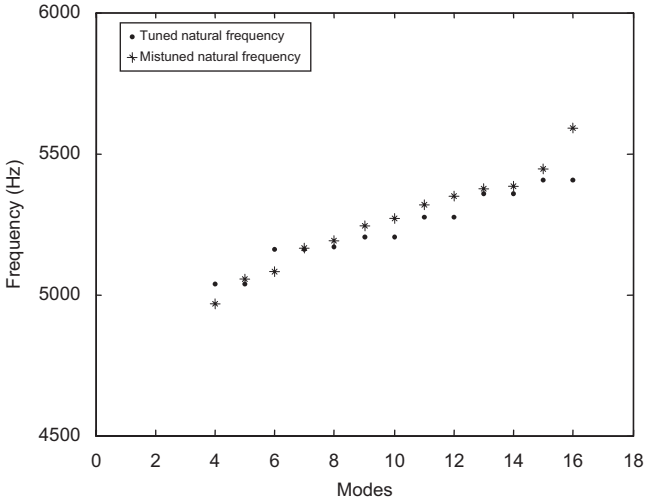

Fig. 5. Tuned (dot) and mistuned (star) natural frequencies of modes 4–16.

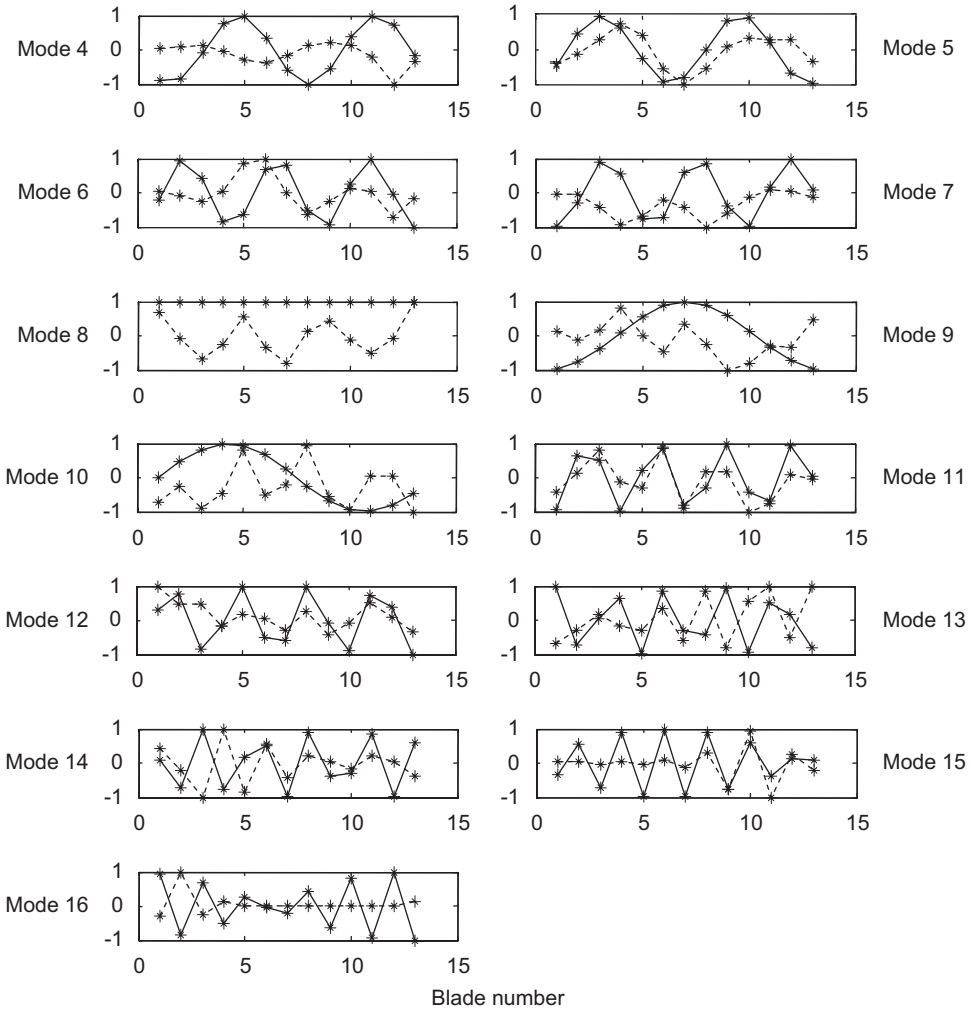

Fig. 6. The 4th to 16th modal shapes of the tuned (—) and mistuned (– – –) wheels in terms of blade tip tangential displacements.

blade mass, the first stage tangential blade stiffness and the blade coupling stiffness of each of 13 blades. Distributions for all the random variables are independent of each other. The mean of each random variable is equal to the corresponding tuned value and the standard deviation equal to 10 percent of the mean. Parameters for the mistuned wheel are listed in Table 2.

Fig. 4 shows the natural frequencies of the tuned (dot) and mistuned (star) wheels. The first mode with a vanishing natural frequency is a rigid mode in which the whole wheel rotates about its axis. The second and third modes are associating with the wheel as a whole vibrating in the x and y directions. Other modes form a pattern of four steps and the tuned modes (of ND numbers 0 to 6) in the first step form the first family of modes. Mistuning does not change this 'step' pattern. The tip-to-tip frequency response matrix $\tilde{\mathbf{H}}(\omega)$ of the mistuned wheel consists of the tangential displacement, observed from the ground, of the second stage blade mass due to a tangential unit force at the second stage mass of the same or other blades. To utilise Eq. (26) for order response predictions, tuned modes in the first family, i.e. modes No. 4 to 16, are employed. The tuned

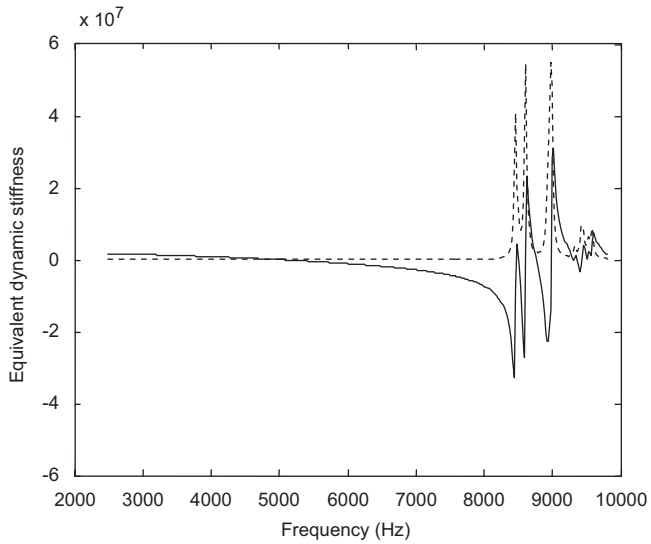

Fig. 7. The 1st element in the equivalent dynamic stiffness matrix of the lumped parameter wheel model: —, real part; and – – –, imaginary part.

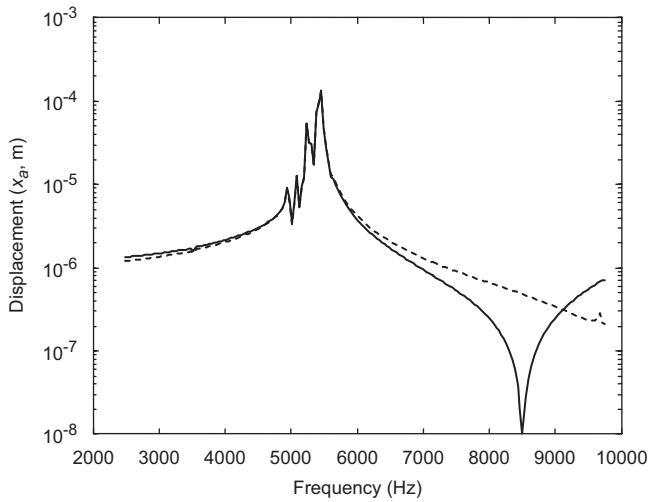

Fig. 8. The 6th order tangential displacement of the 1st mass of the 9th blade: —, Eq. (1); and – – –, Eq. (26).

and mistuned natural frequencies and modal shapes of these modes are shown in Figs. 5 and 6. Fig. 5 shows how the natural frequencies are changed from the tuned ones by mistuning. The modal shapes in Fig. 6 are plotted in terms of the blade tip tangential displacements, with the maximum one being set to be unit. The tuned modes and mistuned modes are significantly different. Vibration localisation (i.e. few neighbouring blades have much greater displacements than others) is observed in the 15th and 16th modes of the mistuned wheel. The first element in the equivalent dynamic stiffness matrix (see Eq. (22)) is shown in Fig. 7. From this it can be concluded that, for frequencies higher than 8 kHz, Eq. (26) cannot be used to predict order responses.

The displacement amplitudes (relative to the disk) of the blade masses of the 9th blade under the 6th order excitation, computed using either Eq. (26) or Eq. (1), is shown in Figs. 8–11. In the order excitation, blade masses are subject to forces only in the tangential direction, as indicated in Eq. (30). The magnitudes of the forces on the 1st and 2nd stage blade masses are 1 and 0.5 N, respectively. It can be seen that, for frequencies around the natural frequencies in the first family of modes of the mistuned wheel, the identified model gives an accurate order response prediction, both in the tangential and radial directions, although the method is based on frequency response functions in the tangential direction. It is particularly important that the maximum

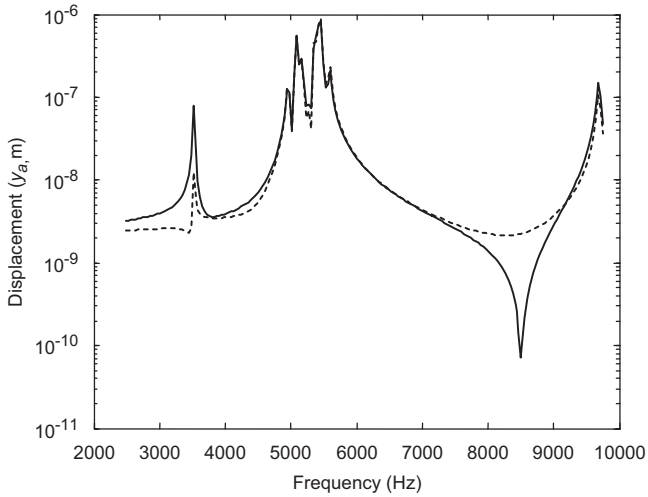

Fig. 9. The 6th order radial displacement of the 1st mass of the 9th blade: —, Eq. (1); and – – –, Eq. (26).

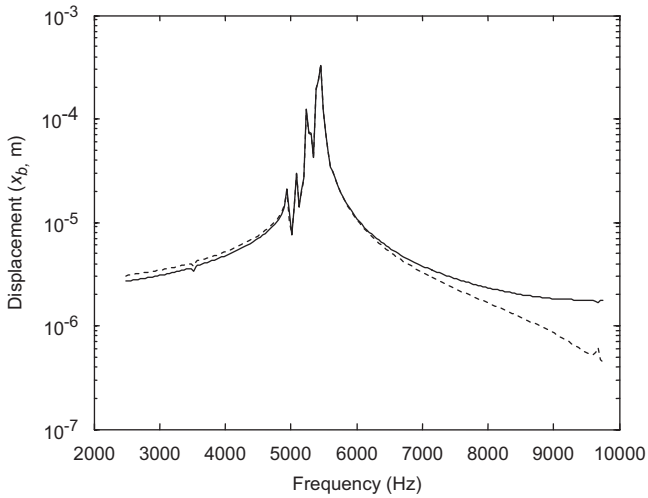

Fig. 10. The 6th order tangential displacement of the 2nd mass of the 9th blade: —, Eq. (1); and – – –, Eq. (26).

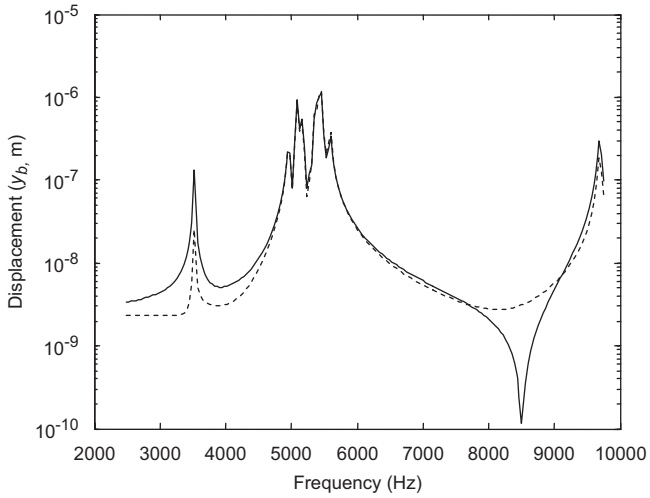

Fig. 11. The 6th order radial displacement of the 2nd mass of the 9th blade: —, Eq. (1); and – – –, Eq. (26).

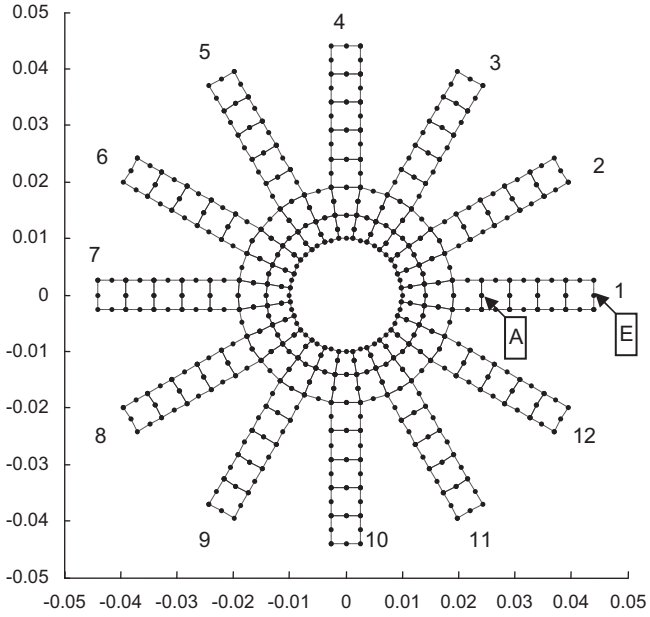

Fig. 12. A paddle wheel and FE mesh in metres.

order response of a blade can be accurately predicted using the identified model. At lower frequencies, the prediction is still good for the tangential displacement. This is not true for the radial displacement. Figs. 9 and 11 show a peak at about 3500 Hz. This corresponds to the second or third mode of the wheel in which the wheel vibrates as a whole translationally on the disk springs. If the wheel is tuned, this mode will not be excited by the 6th order excitation. The chosen tuned modes cannot represent this mode very well, although they generate a peak at the same frequency.

3.2. For a finite element paddle wheel model

Two paddle wheels of 12 blades, one tuned and the other mistuned, are considered and the FE mesh is shown in Fig. 12. The inner and outer radii of the disk are 1 and 1.9 cm. The length and width of each blade

are 2.5 and 0.5 cm. There are five 8-noded elements on each blade. The middle nodes of the elements are identified by A, B, C, D and E as shown in the figure.

For the tuned wheel, Young's modulus is 91 GPa, density is 2783 kg/m^3 and Poisson ratio is 0.33. Since a plane-strain FE program is used, Young's modulus and Poisson ratio have been modified to be 85.5 GPa and 0.248, so that a plane-stress solution is yielded from this FE analysis. For the mistuned wheel, material properties are identical to those of the tuned wheel, except for Young's modulus of the blades; Young's modulus of blade 1–12, is, respectively, 86.53, 90.00, 94.00, 71.90, 84.73, 79.58, 76.65, 74.86, 87.87, 81.73, 85.88 and 82.26 GPa (Fig. 13). They are produced from a normal distribution with the mean being 85.5 GPa and the standard deviation being 10 percent of the mean. A loss factor of 0.005 is used for material damping.

The tip-to-tip frequency response matrix $\tilde{\mathbf{H}}(\omega)$ of the mistuned wheel consists of the tangential (i.e. normal to the blade) displacement of node E on a blade due to a tangential unit force at node E of the same or other blades. In an order excitation, each of nodes A to E is applied a unit force in the tangential direction and these five forces are in-phase. Equivalent nodes on other blades are also forced during an order excitation, but with different phases, as described in Eq. (4).

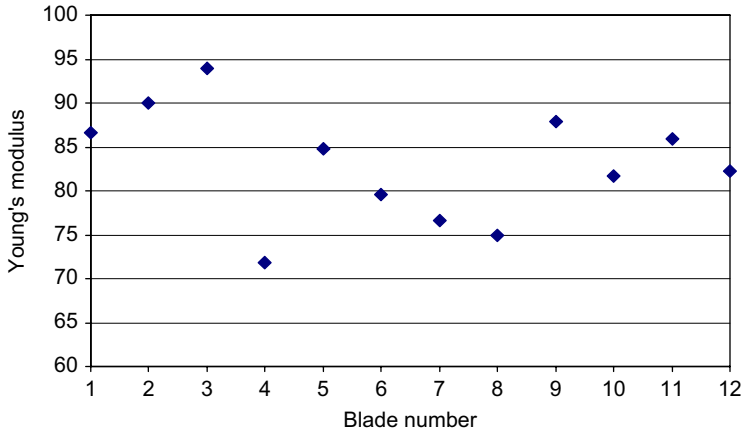

Fig. 13. Blade Young's modulus.

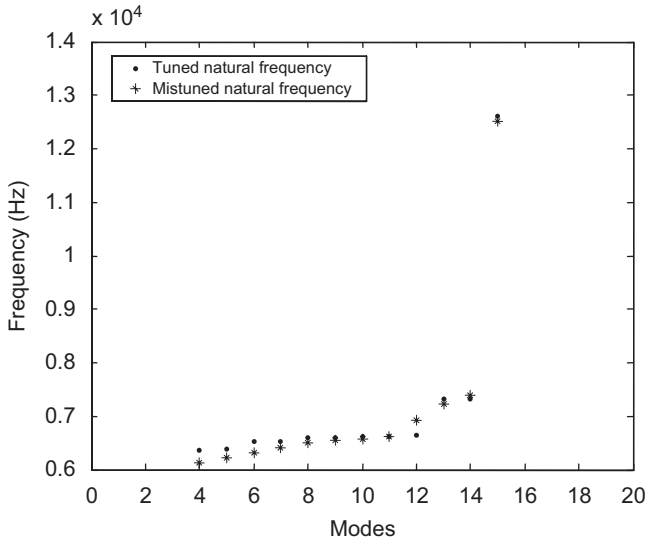

Fig. 14. Natural frequencies of the tuned (dot) and mistuned (star) wheels.

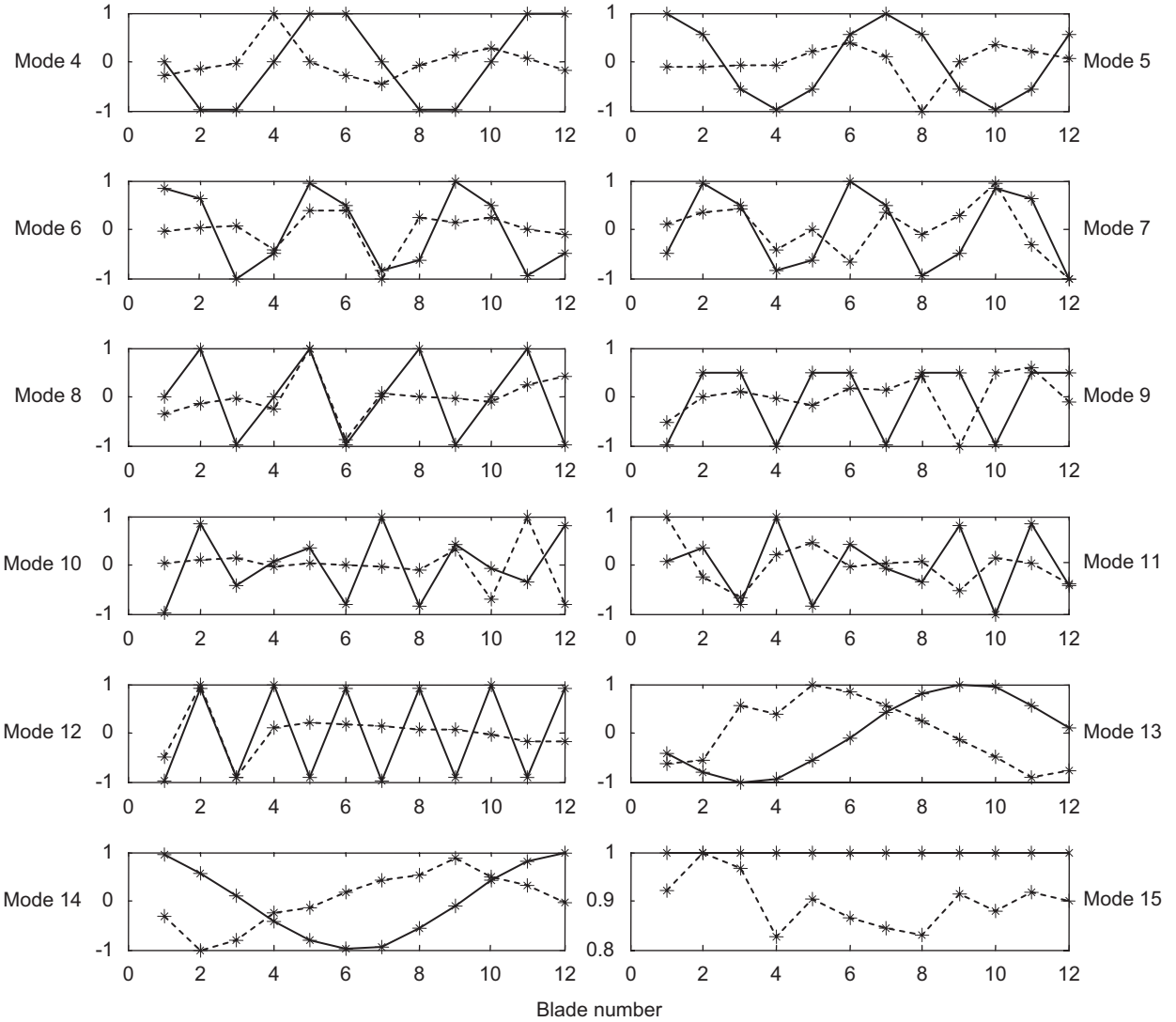

Fig. 15. Modal shapes of the tuned (—) and mistuned (– – –) wheels.

Fig. 14 shows the natural frequencies of the tuned (dot) and mistuned (star) wheels of the first family of modes (modes 4–15. The first three modes are rigid body modes). A huge variation is seen between the natural frequencies of this family (the natural frequency of the 15th mode is much higher than other natural frequencies). Fig. 15 displays the modal shapes in terms of the blade tip (i.e. node E) tangential displacements with the maximum displacement being set to be unit. Vibration localisation is observed in the 10th and 12th modes of the mistuned wheel. The tangential displacement amplitudes of nodes A and E on blade 9 of the mistuned wheel under the 6th order excitation, computed using either Eq. (1) or (26) is shown in Figs. 16 and 17. It can be seen that, the identified model gives an excellent order response prediction for the frequency range spanned by the mistuned natural frequencies of the family.

4. Conclusions

A method is presented in this paper for model identification and order response prediction for mistuned, bladed wheels. This method makes use of measured blade tip-to-blade tip frequency response functions of a mistuned wheel and assumes responses of the wheel subject to order excitations to be a weighted sum of a

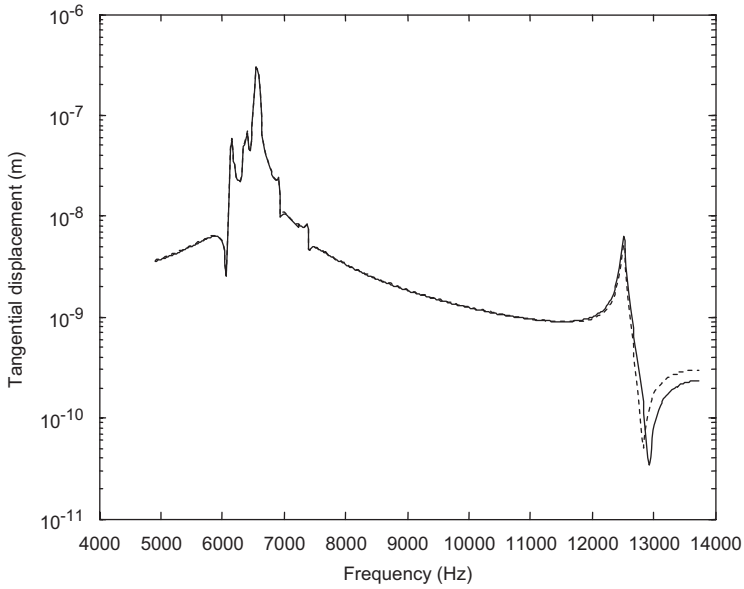

Fig. 16. The 6th order tangential displacement of node A on blade 9: —, Eq. (1); and – – –, Eq. (26).

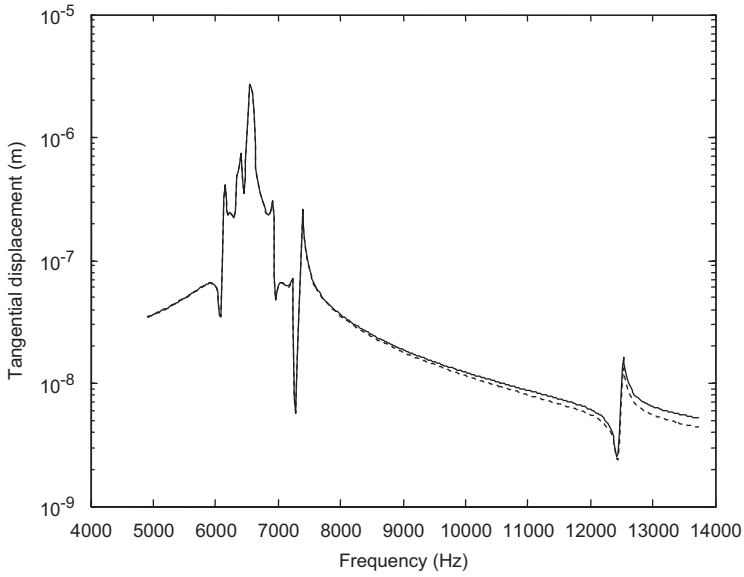

Fig. 17. The 6th order tangential displacement of node E on blade 9: —, Eq. (1); and – – –, Eq. (26).

number, which is equal to the number of the blades, of modes of the corresponding tuned wheel. Order-reduced model for a mistuned wheel is identified in terms of the scale-reduced mass and stiffness matrices from which an expression for order responses is derived. This method is especially suitable for small radial turbocharger turbine wheels.

Order responses of a 10 percent mistuned, lumped parameter wheel model and a 10 percent mistuned, finite element wheel model are calculated using this method and compared with those calculated from the original equation. It is shown that, at and around the natural frequencies of the first family of modes, order responses can be accurately predicted using the proposed method.

Appendix A. Differential equations of motion of the lumped parameter wheel model

The differential equations of motion of the model shown in Fig. A1 are as follows.
For the disk

$$M\ddot{x} + kx + \left(\sum_{j=1}^{N} k_{aj}x_{aj}\,\sin\,\alpha_j\right) - \left(\sum_{j=1}^{N} k_{bj}y_{aj}\,\cos\,\alpha_j\right) = 0, \tag{A.1}$$

$$M\ddot{y} + ky - \left(\sum_{j=1}^{N} k_{aj}x_{aj}\,\cos\,\alpha_j\right) - \left(\sum_{j=1}^{N} k_{bj}y_{aj}\,\sin\,\alpha_j\right) = 0, \tag{A.2}$$

$$J\ddot{\theta} - R_a\sum_{j=1}^{N} k_{aj}x_{aj} = 0. \tag{A.3}$$

For masses m_{aj} and m_{bj} ($j = 1,2,\ldots,N$) (terms with orders higher than one are neglected)

$$\begin{aligned}
&-(m_{aj}\,\sin\,\alpha_j)\ddot{x} + (m_{aj}\,\cos\,\alpha_j)\ddot{y} + m_{aj}R_a\ddot{\theta} + m_{aj}\ddot{x}_{aj}\\
&-\left[k_{e,j-1}\cos^2\frac{\pi}{N}\right]x_{a,j-1} + \left[k_{e,j-1}\,\sin\frac{\pi}{N}\cos\frac{\pi}{N}\right]y_{a,j-1}\\
&+\left[k_{aj} + k_{cj} + (k_{ej} + k_{e,j-1})\cos^2\frac{\pi}{N}\right]x_{aj} - \left[(k_{ej} - k_{e,j-1})\,\sin\frac{\pi}{N}\cos\frac{\pi}{N}\right]y_{aj}\\
&-k_{cj}x_{bj} - \left[k_{ej}\cos^2\frac{\pi}{N}\right]x_{a,j+1} - \left[k_{ej}\,\sin\frac{\pi}{N}\cos\frac{\pi}{N}\right]y_{a,j+1} = P_a e^{\mathrm{i}n\alpha_j}e^{\mathrm{i}\omega t},
\end{aligned} \tag{A.4}$$

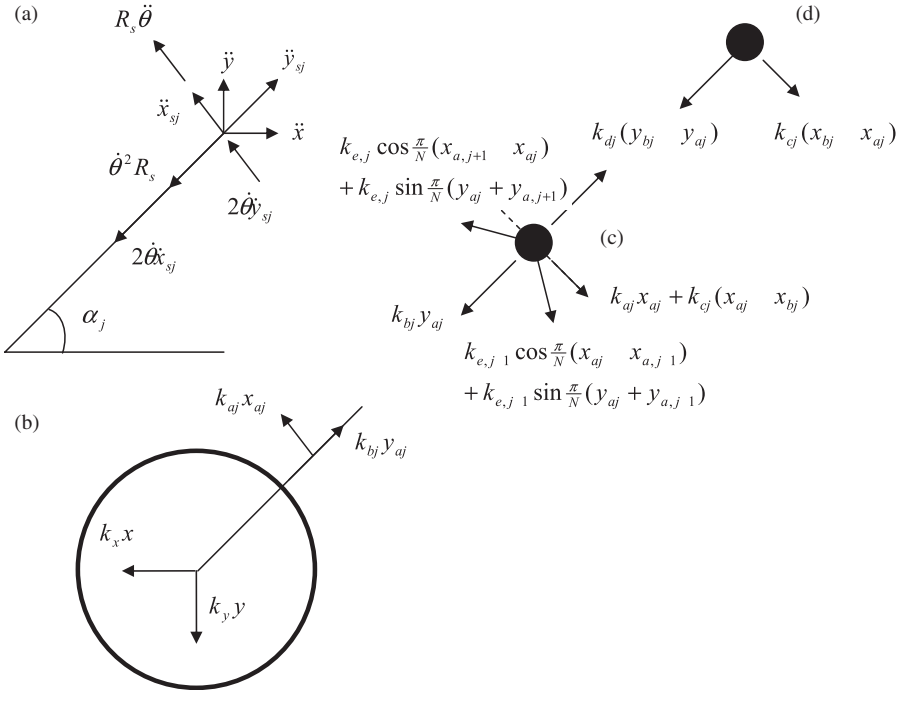

Fig. A1. (a) Accelerations of mass m_{sj}; (b) forces applied on the disk; (c) forces on mass m_{aj}; and (d) forces on mass m_{bj}.

$$(m_{aj}\cos\alpha_j)\ddot{x}+(m_{aj}\sin\alpha_j)\ddot{y}+m_{aj}\ddot{y}_{aj}-\left[k_{e,j-1}\sin\frac{\pi}{N}\cos\frac{\pi}{N}\right]x_{a,j-1}+\left[k_{e,j-1}\sin^2\frac{\pi}{N}\right]y_{a,j-1}+\left[(k_{e,j-1}-k_{ej})\sin\frac{\pi}{N}\cos\frac{\pi}{N}\right]x_{aj}+\left[k_{bj}+k_{dj}+(k_{ej}+k_{e,j-1})\sin^2\frac{\pi}{N}\right]y_{aj}-k_{dj}y_{bj}+\left[k_{ej}\sin\frac{\pi}{N}\cos\frac{\pi}{N}\right]x_{a,j+1}+\left[k_{ej}\sin^2\frac{\pi}{N}\right]y_{a,j+1}=0, \tag{A.5}$$

$$-(m_{bj}\sin\alpha_j)\ddot{x}+(m_{bj}\cos\alpha_j)\ddot{y}+m_{bj}R_b\ddot{\theta}+m_{bj}\ddot{x}_{bj}-k_{cj}x_{aj}+k_{cj}x_{bj}=P_a e^{in\alpha_j}e^{i\omega t}, \tag{A.6}$$

$$(m_{bj}\cos\alpha_j)\ddot{x}+(m_{bj}\sin\alpha_j)\ddot{y}+m_{bj}\ddot{y}_{bj}-k_{dj}y_{aj}+k_{dj}y_{bj}=0. \tag{A.7}$$

References

[1] D.L. Thomas, Dynamics of rotationally periodic structures, *International Journal of Numerical Methods in Engineering* 14 (1979) 81–102.

[2] M. Petyt, *Introduction to Finite Element Vibration Analysis*, Cambridge University Press, Cambridge, 1998.

[3] M.P. Castanier, C. Pierre, Modelling and analysis of mistuned bladed disk vibration: status and emerging directions, *Journal of Propulsion and Power* 22 (2006) 384–396.

[4] D.J. Ewins, The effect of detuning upon the forced vibration of bladed disks, *Journal of Sound and Vibration* 9 (1969) 65–79.

[5] J.H. Griffin, T.M. Hoosac, Model development and statistical investigation of turbine blade mistuning, *ASME Journal of Vibration, Acoustics, Stress and Reliability Design* 106 (1984) 204–210.

[6] A.V. Srinivasan, Flutter and resonant vibration characteristics of engine blades, *ASME Journal of Engineering for Gas Turbine and Power* 119 (1997) 742–775.

[7] R. Bladh, M.P. Castanier, C. Pierre, Component-mode-based reduced order modelling techniques for mistuned bladed disks—part I: theoretical models, *ASME Journal of Engineering for Gas Turbine and Power* 123 (2001) 89–99.

[8] R. Bladh, M.P. Castanier, C. Pierre, Component-mode-based reduced order modelling techniques for mistuned bladed disks—part II: application, *ASME Journal of Engineering for Gas Turbine and Power* 123 (2001) 100–108.

[9] R. Bladh, C. Pierre, M.P. Castanier, M.J. Kruse, Dynamic response predictions for a mistuned industrial turbomachinery rotor using reduced-order modelling, *ASME Journal of Engineering for Gas Turbine and Power* 124 (2002) 311–324.

[10] F. Moyroud, T. Fransson, G. Jacquet-Richardet, A comparison of two finite element reduction techniques for mistuned bladed disks, *ASME Journal of Engineering for Gas Turbine and Power* 124 (2002) 942–952.

[11] S. Lim, R. Bladh, M.P. Castanier, C. Pierre, A compact, generalised component mode mistuning representation for modelling bladed disk vibration, *Proceedings of the AIAA/ASME/ASCE/AHS/ASC Structures, Structural Dynamics and Materials Conference*, Vol. 2, AIAA, New York, 2003, pp. 1359–1380.

[12] E.P. Petrov, K.Y. Sanliturk, D.J. Ewins, A new method for dynamic analysis of mistuned bladed disks based on the exact relationship between tuned and mistuned systems, *ASME Journal of Engineering for Gas Turbine and Power* 124 (2002) 586–596.

[13] D.M. Feiner, J.H. Griffin, A fundamental model of mistuning for a single family of modes, *ASME Journal of Turbomachinery* 124 (2002) 597–605.

[14] A.J. Rivas-Guerra, M.P. Mignolet, J.P. Delor, Identification of mistuning characteristics of bladed disks from free response data—part I, *ASME Journal of Engineering for Gas Turbine and Power* 123 (2001) 395–403.

[15] A.J. Rivas-Guerra, M.P. Mignolet, J.P. Delor, Identification of mistuning characteristics of bladed disks from free response data—part II, *ASME Journal of Engineering for Gas Turbine and Power* 123 (2001) 404–411.

[16] D.M. Feiner, J.H. Griffin, Mistuning identification of bladed disks using a fundamental mistuning model—part I: theory, *ASME Journal of Turbomachinery* 126 (2004) 150–158.

[17] D.M. Feiner, J.H. Griffin, Mistuning identification of bladed disks using a fundamental mistuning model—part II: application, *ASME Journal of Turbomachinery* 126 (2004) 159–165.

[18] O.O. Bendiksen, Localisation phenomena in structural dynamics, *Chaos, Solitons and Fractals* 11 (2000) 1621–1660.

[19] G. ôttarsson, C. Pierre, A transfer matrix approach to free vibration localisation in mistuned bladed assemblies, *Journal of Sound and Vibration* 197 (1996) 589–618.

[20] X. Fang, J. Tang, E. Jordan, K.D. Murphy, Crack induced vibration localisation in simplified bladed-disk structures, *Journal of Sound and Vibration* 291 (2006) 395–418.

[21] M.P. Castanier, C. Pierre, Using intentional mistuning in the design of turbomachinery rotors, *AIAA Journal* 40 (2002) 2077–2086.

[22] M.S. Shahruz, Elimination of vibration localisation in mistuned periodic structures, *Journal of Sound and Vibration* 281 (2005) 452–462.

[23] M. Nikolic, E.P. Petrov, D.J. Ewins, Coriolis forces in forced response analysis of mistuned bladed disks, *ASME Journal of Turbomachinery* 129 (2007) 730–739.
[24] D.J. Ewins, *Modal Testing: Theory and Practice*, Research Studied Press Ltd., UK, 1994.
[25] X. Sheng, D.C. Clay, J. Allport, Dynamics of mistuned radial turbine wheels, *Proceedings of the Eighth International Conference on Turbochargers and Turbocharging*, London, England, 2006.